



**HAL**  
open science

# Normal vs. Inverted Ordering of Reduction Potentials in [FeFe]-Hydrogenases Biomimetics: Effect of the Dithiolate Bulk

Federica Arrigoni, Luca de Gioia, Catherine Elleouet, François Pétilion, Philippe Schollhammer, Jean Talarmin, Giuseppe Zampella

## ► To cite this version:

Federica Arrigoni, Luca de Gioia, Catherine Elleouet, François Pétilion, Philippe Schollhammer, et al.. Normal vs. Inverted Ordering of Reduction Potentials in [FeFe]-Hydrogenases Biomimetics: Effect of the Dithiolate Bulk. *Chemistry - A European Journal*, 2023, 10.1002/chem.202300569 . hal-04108528

**HAL Id: hal-04108528**

<https://hal.science/hal-04108528v1>

Submitted on 11 Oct 2024

**HAL** is a multi-disciplinary open access archive for the deposit and dissemination of scientific research documents, whether they are published or not. The documents may come from teaching and research institutions in France or abroad, or from public or private research centers.

L'archive ouverte pluridisciplinaire **HAL**, est destinée au dépôt et à la diffusion de documents scientifiques de niveau recherche, publiés ou non, émanant des établissements d'enseignement et de recherche français ou étrangers, des laboratoires publics ou privés.



Distributed under a Creative Commons Attribution 4.0 International License

# Normal vs. Inverted Ordering of Reduction Potentials in [FeFe]-Hydrogenases Biomimetics: Effect of the Dithiolate Bulk

Federica Arrigoni,<sup>\*[b]</sup> Luca De Gioia,<sup>[b]</sup> Catherine Elleouet,<sup>\*[a]</sup> François Y. Pétilion,<sup>[a]</sup> Philippe Schollhammer,<sup>\*[a]</sup> Jean Talarmin,<sup>[a]</sup> and Giuseppe Zampella<sup>\*[b]</sup>

**Abstract:** Three hexacarbonyl diiron dithiolate complexes [Fe<sub>2</sub>(CO)<sub>6</sub>(μ-(SCH<sub>2</sub>)<sub>2</sub>X)] with different substituted bridgeheads (X=CH<sub>2</sub>, CEt<sub>2</sub>, CBn<sub>2</sub> (Bn=CH<sub>2</sub>C<sub>6</sub>H<sub>5</sub>)), have been studied under the same experimental conditions by cyclic voltammetry in dichloromethane [NBu<sub>4</sub>][PF<sub>6</sub>] 0.2 M. DFT calculations were performed to rationalize the mechanism of reduction of these compounds. The three complexes undergo a two-electron transfer whose the mechanism depends on the bulkiness of the dithiolate bridge, which involves a different timing of the

structural changes (Fe–S bond cleavage, inversion of conformation and CO bridging) vs redox steps. The introduction of a bulky group in the dithiolate linker has obviously an effect on normally ordered (as for propanedithiolate (pdt)) or inverted (pdt<sup>Et2</sup>, pdt<sup>Bn2</sup>) reduction potentials. Et→Bn replacement is not theoretically predicted to alter the geometry and energy of the most stable mono-reduced and bi-reduced forms but such a replacement alters the kinetics of the electron transfer vs the structural changes.

## Introduction

Multielectron transfers are ubiquitous in biologically important activation processes such as hydrogen production/uptake, nitrogen fixation, or CO<sub>2</sub> reduction, as well as in the catalysis of these reactions.<sup>[1–20]</sup> When compounds reduce in two steps, to the anion and then to the dianion, the second reduction is expected to take place at a more negative potential than the first one due to the electrostatic repulsion. This means that the formal potentials,  $E^{\circ}_1$  and  $E^{\circ}_2$  respectively, follow the “normal ordering of potentials” viz  $E^{\circ}_1 - E^{\circ}_2 > 0$  and this implies that the one-electron intermediate is stable towards the disproportionation.<sup>[21–22]</sup> In cyclic voltammetry, the second electron transfer is occasionally masked because it is situated fairly close to the solvent background limit but in many cases

two sequential one-electron systems can be observed and are separated according to the normal ordering of redox potentials.<sup>[21]</sup> When the difference between the two potentials is very small, the situation is called “potential compression”.<sup>[22,23]</sup> The situation called “potential inversion” corresponds to the case where the second electron transfer is easier than the first one.<sup>[16–32]</sup> The conditions under which the two electron transfers of such EE systems can be kinetically discriminated were reported.<sup>[33–35]</sup> The influence of molecular and medium effects on the two-electron processes have been investigated in detail.<sup>[22–42]</sup> The potential inversion can be the consequence of a structural change, an electronic relaxation (intrinsic factors) or the result of the solvation or the formation of ion-pairing (extrinsic factors). Since the potential inversion may be favoured by a structural change, it is not surprising at first glance that sluggish electron transfer kinetics is observed when important structural changes occur. Conversely, high-rate constants are expected to be found when structural changes are minimal. Nevertheless, a large potential inversion will also bring a system to behave less reversibly than it would with normal ordering of potentials, which means that the electron transfer kinetics appears more sluggish. This is known as the burden kinetic effect.<sup>[24]</sup> The magnitude of this effect depends upon the standard rate constants. It is worth noting that besides the heterogeneous electron transfers, disproportionation (or comproportionation) reaction in diffusion layer has sometimes to be considered to analyse and understand the shape of the curves obtained in cyclic voltammetry. But if disproportionation (Disp) occurs, it has no effect on the shape of the cyclic voltammogram when the first electron transfer is the determining rate step.<sup>[37]</sup> When the rate constants are high, a concerted EE mechanism can be only considered. For potential inversion greater than 300 mV, disproportionation is not relevant.<sup>[42]</sup>

[a] Dr. C. Elleouet, Prof. Emeritus Dr. F. Y. Pétilion, Prof. Dr. P. Schollhammer, Dr. J. Talarmin  
UMR CNRS 6521 Chimie, Electrochimie Moléculaires et Chimie Analytique  
Université de Bretagne Occidentale, UFR Sciences et Techniques  
6 Avenue Victor le Gorgeu, CS 93837, 29238 Brest-Cedex 3 (France)  
E-mail: catherine.elleouet@univ-brest.fr  
philippe.schollhammer@univ-brest.fr

[b] Dr. F. Arrigoni, Prof. Dr. L. De Gioia, Prof. Dr. G. Zampella  
Department of Biotechnology and Bioscience  
University of Milano-Bicocca  
Piazza della Scienza 2, 20126 Milan (Italy)  
E-mail: federica.arrigoni@unimib.it  
giuseppe.zampella@unimib.it

Supporting information for this article is available on the WWW under <https://doi.org/10.1002/chem.202300569>

© 2023 The Authors. Chemistry - A European Journal published by Wiley-VCH GmbH. This is an open access article under the terms of the Creative Commons Attribution Non-Commercial NoDerivs License, which permits use and distribution in any medium, provided the original work is properly cited, the use is non-commercial and no modifications or adaptations are made.

Otherwise, when a first transfer of electron triggers a chemical reaction (ligand binding or loss, 'parent-child' reaction, protonation etc.), the resulting product might be easier to reduce than the initial complex, and a second electron might be transferred at the same potential as the first, through a classical ECE process.<sup>[43,44]</sup>

As suggested above, one of the difficulties in the interpretation of the two-electron processes arises from the fact that cyclic voltammograms may be very similar while they represent different combinations of criterions depending on whether the electron transfers are separated (ECE mechanism) or concerted (EE mechanism) and whether the dominant structural change is coupled to the first or the second electron transfer. In the case of an ECE-Disp process, the second electron transfer may have several possible sources since the rate determining step may be the chemical reaction or the disproportionation reaction.<sup>[45]</sup> Moreover additional competitive reactions may arise.

Numerous works describing the electrochemical behaviour of diiron dithiolate compounds as models of hydrogenase enzymes, which produce or consume H<sub>2</sub>, are found in the literature. Such diiron species are perfect candidates to perform the transfer of two electrons. Some diiron dithiolate compounds, with electron-withdrawing bridges, reduce in two sequential one-electron steps.<sup>[46–49]</sup> Combined sequential one-electron transfers and ECE process have been also reported.<sup>[50]</sup> Single step two-electron reduction processes due to potential inversion have been observed in several instances for hexacarbonyl diiron dithiolate, as well as for diselenolate or diphosphide, complexes.<sup>[49–77]</sup>

In this work, a series of hexacarbonyl diiron dithiolate compounds, carrying differently crowded bridgeheads, is studied under identical experimental conditions. Thus, the electrochemical studies of the reduction of [Fe<sub>2</sub>(CO)<sub>6</sub>(μ-(SCH<sub>2</sub>)<sub>2</sub>X)] complexes with X=CET<sub>2</sub><sup>[78]</sup> and X=CBn<sub>2</sub> (Bn=CH<sub>2</sub>C<sub>6</sub>H<sub>5</sub>) were carried out in dichloromethane in the presence of the supporting electrolyte [NBu<sub>4</sub>][PF<sub>6</sub>] at 0.2 M. For the sake of comparison, the electrochemical investigation in CH<sub>2</sub>Cl<sub>2</sub>-[NBu<sub>4</sub>][PF<sub>6</sub>] 0.2 M of the reduction of the propanedithiolate (X=CH<sub>2</sub>) complex, which was previously studied in other electrolytic solutions,<sup>[54,79–81]</sup> was also performed. It is known that the nature of the solvent as well as the supporting electrolyte may strongly affect the potentials of redox couples and thus, the electron stoichiometry of multielectron processes.<sup>[26,27,82–88]</sup> DFT calculations were performed with the aim of elucidating the mechanistic details characterising the reduction of the diiron complexes under investigation.

## Results and Discussion

### Synthesis and characterization of compounds [Fe<sub>2</sub>(CO)<sub>6</sub>(μ-(SCH<sub>2</sub>)<sub>2</sub>X)] (X=CH<sub>2</sub> (1), CET<sub>2</sub> (2), CBn<sub>2</sub> (3))

The synthesis and the characterization of compounds 1, 2 were previously reported.<sup>[78,79,89,90]</sup> The procedure for the preparation of 3 and its spectroscopic data (IR, <sup>1</sup>H NMR) have not been yet reported. They are described in the experimental part. Single

crystals of 3, suitable for X-ray crystallography, were grown upon slow diffusion of hexane into dichloromethane solution of 3 at –20 °C. The ORTEP view of 3 and selected X-ray data are shown in Figure 1. The solid state structure of 3 is very close to that of other diiron hexacarbonyl dithiolato complexes with steric bulky bridge-head substituents.<sup>[78]</sup> Typically, a torsion angle, C4-Fe2-Fe1-C1 (OC<sub>ap</sub>-Fe-Fe-CO<sub>ap</sub>) of ~11.5° reveals a slight distortion between the two {Fe(CO)<sub>3</sub>} moieties due to the steric crowding of the benzyl substituents. The difference of the two bonds angles Fe1C1O1 and Fe2C4O4, of 174.4(4)° and 177.8(4)°, respectively, is also noticeable and related to a possible weak interaction C–H...C<sub>ap</sub>–Fe between the CH<sub>2</sub> group of a benzyl substituent and one apical FeCO bond (C1...H10b ~2.41 Å).

### Electrochemistry of compounds [Fe<sub>2</sub>(CO)<sub>6</sub>(μ-(SCH<sub>2</sub>)<sub>2</sub>X)] (X=CH<sub>2</sub> (1), CET<sub>2</sub> (2), CBn<sub>2</sub> (3))

#### Under Ar

One of the goals of the electrochemical study was to determine the number of electrons involved in the reduction processes of the complexes 1–3. For this purpose, the scan rate (*v*) dependences of the current function (*i<sub>p</sub>*/(*v*<sup>1/2</sup>*C*; *C* is the concentration of the complex)<sup>[91]</sup> for the reduction of the complexes have been compared with that of a reference compound, [Fe<sub>2</sub>(CO)<sub>4</sub>(κ<sup>2</sup>-LL)(μ-(SCH<sub>2</sub>)<sub>2</sub>CH<sub>2</sub>)] (LL=I<sub>Me</sub>-CH<sub>2</sub>-I<sub>Me</sub>, I<sub>Me</sub>=1-methylimidazol-2-ylidene), previously shown to undergo a partially reversible one-electron oxidation in CH<sub>2</sub>Cl<sub>2</sub>-[NBu<sub>4</sub>][PF<sub>6</sub>].<sup>[92]</sup>

The shape of the cyclic voltammograms of the complex [Fe<sub>2</sub>(CO)<sub>6</sub>(μ-(SCH<sub>2</sub>)<sub>2</sub>CH<sub>2</sub>)] (1) in CH<sub>2</sub>Cl<sub>2</sub>-[NBu<sub>4</sub>][PF<sub>6</sub>] is strongly

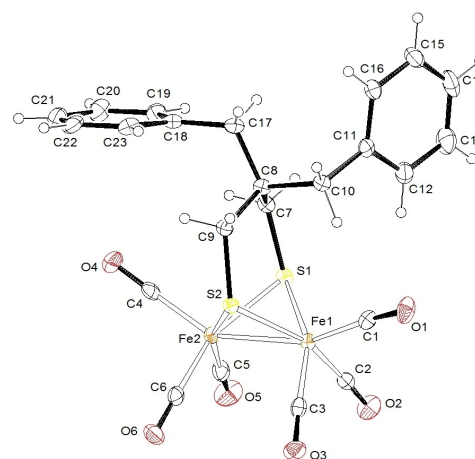


**Figure 1.** Ortep view (ellipsoids at 30% of probability level) of 3. Selected distances (Å) and angles (deg): Fe1-Fe2, 2.4966(8); S1-Fe1, 2.2667(12); S1-Fe2, 2.2616(12); S2-Fe2, 2.2492(13); S2-Fe1, 2.2587(12); C1-O1, 1.140(5); C1-Fe1, 1.781(5); C2-O2, 1.151(5); C2-Fe1, 1.799(5); C3-O3, 1.133(5); C3-Fe1, 1.790(5); C4-O4, 1.143(5); C4-Fe2, 1.808(5); C5-O5, 1.134(5); C5-Fe2, 1.802(5); C6-O6, 1.147(5); C6-Fe2, 1.797(5); Fe1-S1-Fe2, 66.92(3); Fe2-S2-Fe1, 67.26(4); C1-Fe1-Fe2, 157.49(13); C4-Fe2-Fe1, 147.19(13); O1-C1-Fe1, 174.4(4); O2-C2-Fe1, 177.7(4); O3-C3-Fe2, 176.6(4); O4-C4-Fe2, 177.8(4); O5-C5-Fe2, 178.2(4); O6-C6-Fe2, 178.4(4).

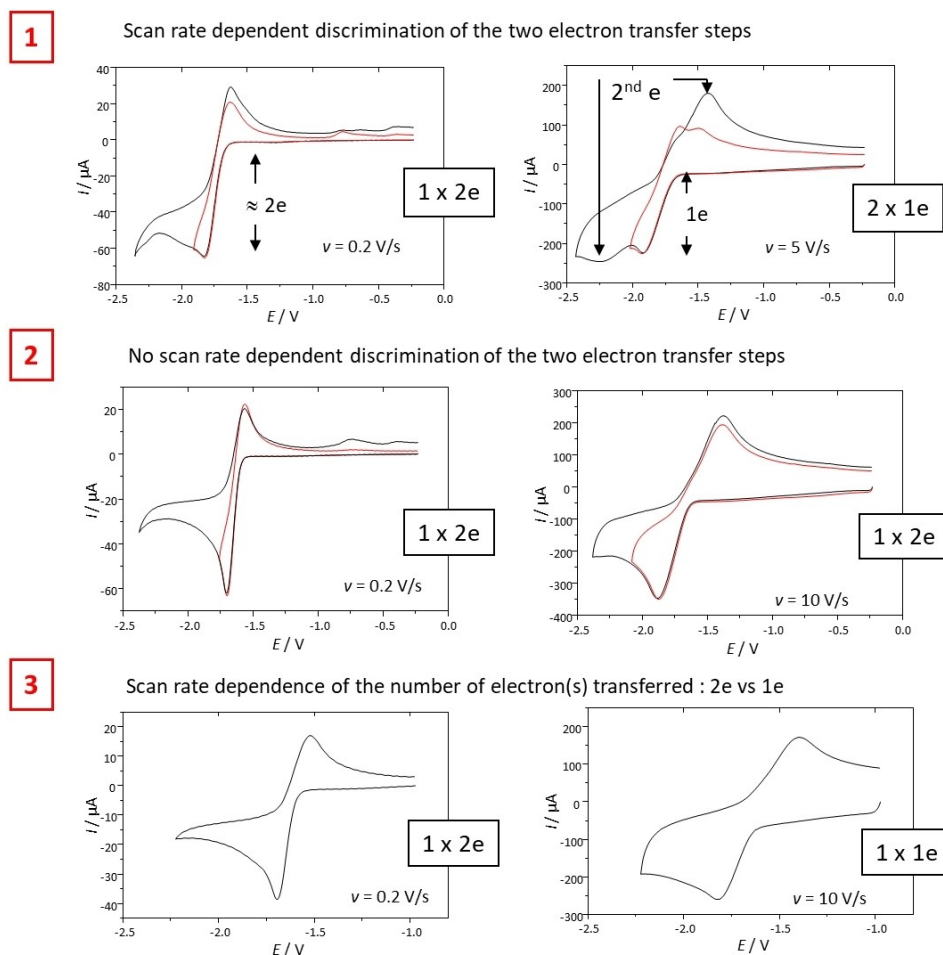


**Figure 2.** Cyclic voltammetry of **1** (1.53 mM), **2** (1.11 mM) and **3** (1.13 mM) at a slow scan rate (left) and a fast scan rate (right) under Ar in  $\text{CH}_2\text{Cl}_2$ - $[\text{NBu}_4][\text{PF}_6]$  (vitreous carbon electrode, potentials are in V vs  $\text{Fc}^+/\text{Fc}$ ).

dependent on the scan rate (Figure 2 and Figure S1, Supporting Information). At very slow scan rates, the reduction occurs according to a partially reversible process whose current is more than twice that of a diffusion-controlled, reversible one-electron transfer. This is shown by the comparison of the current function for the reduction of **1** to that of  $[\text{Fe}_2(\text{CO})_4(\kappa^2\text{-LL})(\mu\text{-}(\text{SCH}_2)_2\text{CH}_2)]$  (Figure 3A).<sup>[93]</sup> Upon increasing the scan rate ( $v \geq 5 \text{ V s}^{-1}$ ), the current function of the first reduction peak decreases and tends towards that corresponding to a one-electron process. Under these conditions, the two successive one-electron reductions of **1** are distinctly observed (Figure 2 right and Figure S1). There is apparently a substantial potential compression since  $E_{1/2}^{\text{red}2}$  is only about 20 mV more negative than  $E_{1/2}^{\text{red}1}$  at low scan rates (see Table 1) but a discriminated potential inversion may not be excluded. Whatever it is, the disproportionation equilibrium constant ( $K_{\text{Disp}}$ ) would be inexistent or low (for information, a value of  $2.4 \cdot 10^{-3}$  has been determined in  $\text{MeCN}-[\text{NBu}_4][\text{PF}_6]$  0.2 M<sup>[54]</sup>). The reduction of **1** is more chemically reversible at very slow scan rates ( $v \leq 0.2 \text{ V s}^{-1}$ ) in  $\text{CH}_2\text{Cl}_2$ - $[\text{NBu}_4][\text{PF}_6]$  than in  $\text{MeCN}-[\text{NBu}_4][\text{PF}_6]$ <sup>[54]</sup> or  $\text{MeCN}-[\text{NBu}_4][\text{BF}_4]$ .<sup>[75,88]</sup> Nevertheless, the fact that the peak current ratio,  $(i_p^a/i_p^c)^{\text{red}}$ , is less than unity (0.74 for  $v=0.05 \text{ V s}^{-1}$ ;

**Table 1.** Reduction potentials of **1–3** in  $\text{CH}_2\text{Cl}_2$ - $[\text{NBu}_4][\text{PF}_6]$ .

Complex	Scan rate [ $\text{V s}^{-1}$ ]	$E_{1/2}^{\text{red}1}$ [V vs $\text{Fc}^+/\text{Fc}$ ]	$\Delta E_p^{\text{red}1}$ [mV]	$E_{1/2}^{\text{red}2}$ [V vs $\text{Fc}^+/\text{Fc}$ ]	$\Delta E_p^{\text{red}2}$ [mV]
<b>1</b>	0.1	−1.73	162	−1.75	470
	1	−1.76	194	−1.79	515
	10	−1.79	370	−1.84	950
<b>2</b>	0.1	−1.63	100	–	–
	1	−1.63	240	–	–
	10	−1.63	500	–	–
<b>3</b>	0.1	−1.61	133	–	–
	1	−1.61	211	–	–
	10	−1.61	426	–	–

0.88 for  $v=0.2 \text{ V s}^{-1}$ <sup>[94]</sup>) and the presence of small oxidation peaks detected at  $-0.78 \text{ V}$  and  $-0.37 \text{ V}$  on the reverse scan (Figure 2 (left) and S1) suggest that the reduced species may not be indefinitely stable in the dichloromethane electrolytic solution.

The cyclic voltammetry of **2** in  $\text{CH}_2\text{Cl}_2$ - $[\text{NBu}_4][\text{PF}_6]$  shows that this complex undergoes one reduction (Figure 2) and two oxidation steps (see Figure S2). Remarkably, the first oxidation at  $E_{1/2}=0.75 \text{ V}$  presents the characteristics of a partially reversible one-electron process at moderate to fast scan rates

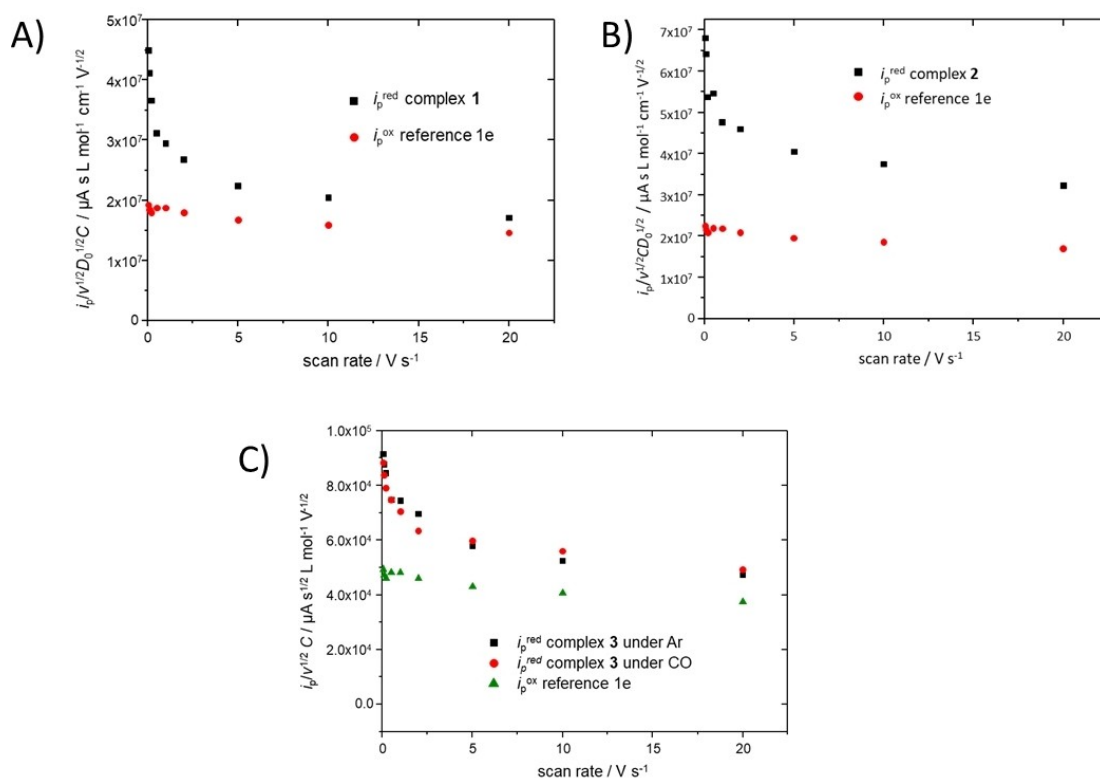


**Figure 3.** A) Scan rate dependence of the current functions for the first reduction of **1** (1.53 mM, black square) and for the reversible, one-electron oxidation of  $[\text{Fe}_2(\text{CO})_4(\kappa^2\text{-LL})(\mu\text{-}(\text{SCH}_2)_2\text{CH}_2)]$  (1.11 mM, red dot) in  $\text{CH}_2\text{Cl}_2\text{-}[\text{NBu}_4][\text{PF}_6]$ . B) Scan rate dependence of the current functions for the reduction of **2** (2.08 mM, black square), and for the reversible, one-electron oxidation of  $[\text{Fe}_2(\text{CO})_4(\kappa^2\text{-LL})(\mu\text{-}(\text{SCH}_2)_2\text{CH}_2)]$  (1.11 mM, red dot) in  $\text{CH}_2\text{Cl}_2\text{-}[\text{NBu}_4][\text{PF}_6]$ . C) Scan rate dependence of the current functions for the reduction of **3** (1.13 mM) under Ar (black square) or CO (red dot) and for the reversible, one-electron oxidation of  $[\text{Fe}_2(\text{CO})_4(\kappa^2\text{-LL})(\mu\text{-}(\text{SCH}_2)_2\text{CH}_2)]$  (1.11 mM, green triangle) in  $\text{CH}_2\text{Cl}_2\text{-}[\text{NBu}_4][\text{PF}_6]$ .

( $v \geq 2 \text{ V s}^{-1}$ , Figure S2, red trace, and Figure S3). The ratio of the reduction peak current to the oxidation one ( $i_p^{\text{red}}/i_p^{\text{ox}}$ ) measured at  $v \geq 2 \text{ V s}^{-1}$  suggests that two electrons are involved in the single reduction step at  $E_{1/2} = -1.63 \text{ V}$  (Figure 2 and Table 1). The decrease of the ratio with lower scan rates arises from the fact that the oxidation of **2** is a multi-electron process at slow scan rates (Figure S3). The comparison of the current function for the reduction of **2** and for the reversible one-electron oxidation of  $[\text{Fe}_2(\text{CO})_4(\kappa^2\text{-LL})(\mu\text{-}(\text{SCH}_2)_2\text{CH}_2)]$  confirms that the former involves two electrons for  $v \geq 2 \text{ V s}^{-1}$ . Notably, at the slowest scan rates, the current measured for the reduction of **2** is more than twice that corresponding to the one-electron oxidation of  $[\text{Fe}_2(\text{CO})_4(\kappa^2\text{-LL})(\mu\text{-}(\text{SCH}_2)_2\text{CH}_2)]$  (Figure 3B). Earlier CV simulations, showing that the ratio (R) of the current of a single reversible two-electron step to the current of a reversible one-electron transfer could be much larger than two, depending on the extent of the potential inversion ( $R \approx 2.7$  for  $E_2^{\text{ox}} - E_1^{\text{red}} = 0.15 \text{ V}$ ) have been reported.<sup>[95]</sup> However, the substantial increase of the current function for the reduction of **2** at slow scan rates may also suggest that an additional, unidentified electron transfer occurs under these conditions.

The cyclic voltammetry of **3** in  $\text{CH}_2\text{Cl}_2\text{-}[\text{NBu}_4][\text{PF}_6]$  (Figure 2) shows that this complex undergoes a quasi-reversible reduction and an irreversible oxidation (not shown). The comparison of the peak currents as well as the current functions (Figure 3C) of

the reduction of **3** with those of the oxidation of the reference compound  $[\text{Fe}_2(\text{CO})_4(\kappa^2\text{-LL})(\mu\text{-}(\text{SCH}_2)_2\text{CH}_2)]$  at different scan rates indicates that the former transitions from a two-electron (slow scan rates) to a one-electron process (fast scan rates), which is consistent with an ECE-type mechanism.

#### Under CO

The presence of CO does not appreciably affect the reduction forward peak current ( $i_p^{\text{c, red}}$ ) of **1** in  $\text{CH}_2\text{Cl}_2\text{-}[\text{NBu}_4][\text{PF}_6]$  (Figure 4) but, on the other hand, the backward peak current is smaller under CO than under Ar which indicates that the dianion reacts with CO to generate a species reversibly oxidised at  $E_{1/2} = -0.66 \text{ V}$  (Figure 4). This result is different to that observed in MeCN<sup>[54,79]</sup> and in DMF<sup>[96]</sup> where the presence of CO improves the chemical reversibility of the reduction of **1**, suggesting a reversible loss of CO during this process. As for **1**, the reduction peak current of **2** and **3** under CO in  $\text{CH}_2\text{Cl}_2\text{-}[\text{NBu}_4][\text{PF}_6]$  is only marginally affected whereas the backward peak is slightly diminished, showing that the dianion reacts with carbon monoxide (Figure S4). On the reverse scan, a reversible oxidation is present at a potential very similar to that observed in the case of complex **1** (at  $E_{1/2} = -0.64 \text{ V}$  for **3**,  $E_{1/2} = -0.66 \text{ V}$  in the case of **1** and **2**). These observations suggest a similar

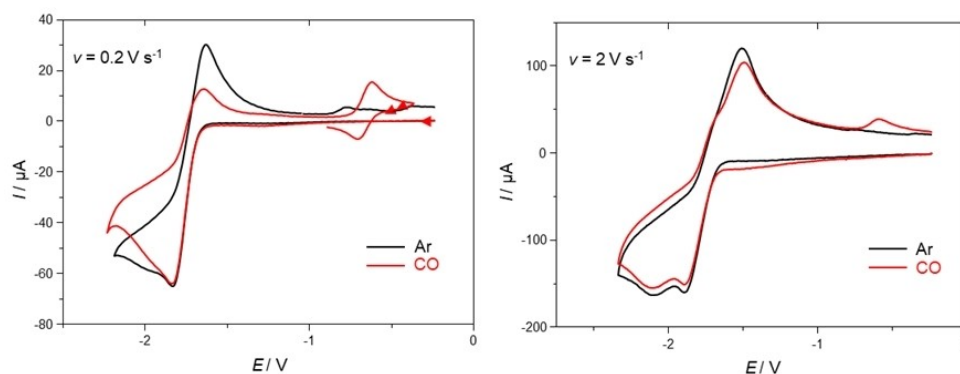


**Figure 4.** Cyclic voltammetry of **1** (1.53 mM) at  $0.2 \text{ V s}^{-1}$  (left) and  $2 \text{ V s}^{-1}$  (right) under Ar (black trace) and under CO (red trace) in  $\text{CH}_2\text{Cl}_2\text{-[NBu}_4\text{][PF}_6\text{]}$  (vitreous carbon electrode, potentials are in V vs  $\text{Fc}^+/\text{Fc}$ ).

behaviour of **2** and **3** towards CO in reduction<sup>[97]</sup> and that the nature of the substituents of the bridge-head C atom affects the kinetics of this process.

#### Rationalization of the electrochemical processes by DFT calculations

The examination by DFT of the thermodynamic speciation of complexes **1–3** in their neutral, anionic and di-anionic forms was performed in order to highlight the effect of the replacement of the bridgehead  $\text{CH}_2\text{-CET}_2\text{-CBn}_2$  in the dithiolate bridge on the stability of the reduced species and thus on the reductive behaviours of compounds **1–3**. For the complex **1** (Figure 5), the study supports previous theoretical investigations suggesting that the first reduction takes place with a geometry retention, followed by a significant structural rearrangement involving a Fe–S breaking and the bridging of one carbonyl group upon the second reduction.<sup>[54,98]</sup> The most stable mono-

anion **1a<sup>-</sup>** exhibits a lengthening of the distance Fe–Fe, 2.859 Å compared to 2.531 Å in **1**, and the geometry remains identical to that of the neutral complex. It is worth noting that the free energy gap between rotated and unrotated isomers (**1b<sup>-</sup>** vs **1a<sup>-</sup>**) is halved (4.2 kcal/mol) compared to that calculated for the neutral complex (9.6 kcal/mol). While isomers with a broken Fe–S bond are strongly disfavoured at the mono-anionic level ( $\Delta G = +15.4 \text{ kcal/mol}$ ), the most stable doubly-reduced species features a broken Fe–S bond and a  $\mu\text{-CO}$  ligand. Two di-anionic isomers (**1a<sup>2-</sup>** and **1b<sup>2-</sup>**) are very close in energy (2.3 kcal/mol), differing only by the conformation of the remaining  $\text{FeS}_2\text{C}_3$  ring. The di-anionic isomer with broken Fe–Fe and preserved Fe–S bonds, **1c<sup>2-</sup>**, is 8.5 kcal/mol less stable than the ground state.

Three conformers were characterised for the neutral form of complexes **2** and **3** (Figures 6 and S5 respectively). The introduction of two R substituents ( $\text{R}=\text{Et}$  or  $\text{Bn}$ ) on the bridge head carbon atom generates the possibility to observe two, nearly energetically equivalent, isomers ( $\Delta G = 1.3 \text{ kcal/mol}$  and  $0.7 \text{ kcal/mol}$  for **2** and **3**, respectively) differing by syn/anti

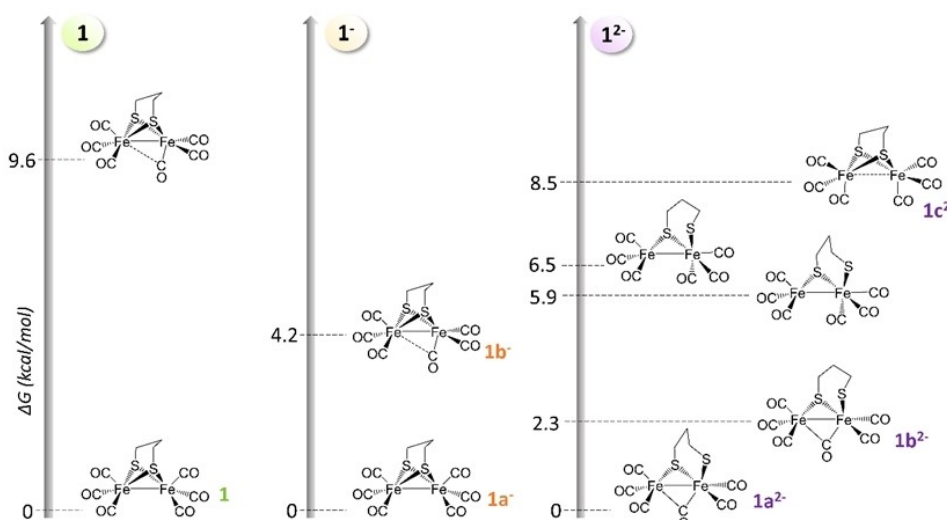


**Figure 5.** Thermodynamic speciation of **1**, **1<sup>-</sup>** and **1<sup>2-</sup>**. Highly unstable isomers (i.e.,  $\Delta G > 10 \text{ kcal/mol}$ ) are not displayed in this case (see text).

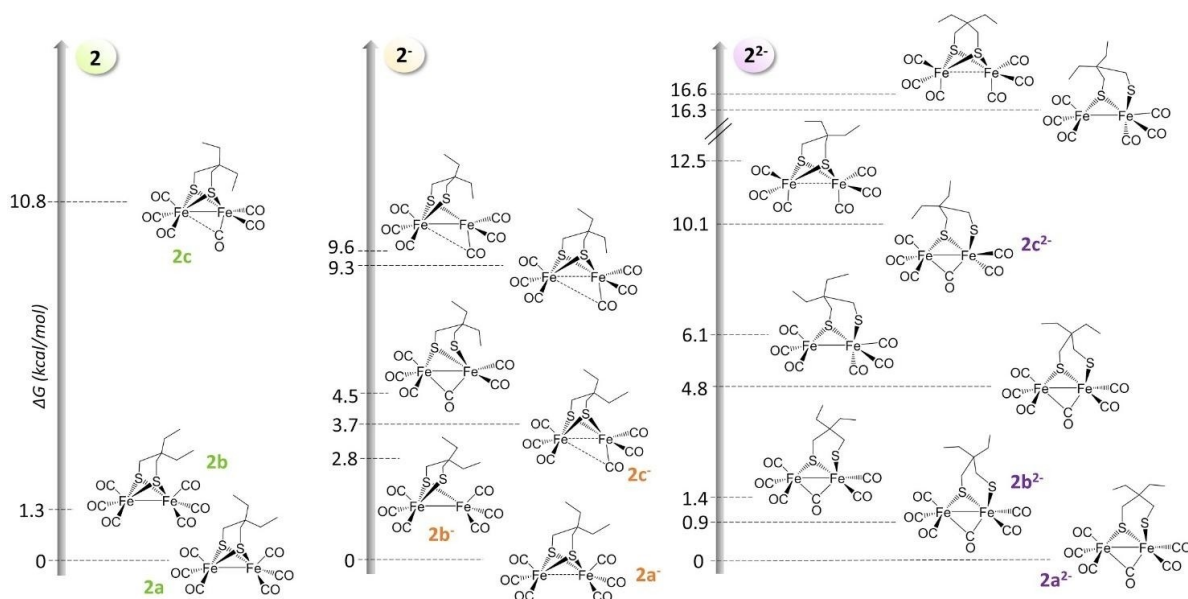


Figure 6. Most relevant isomers resulting from the thermodynamic speciation of  $2$ ,  $2^-$  and  $2^{2-}$  (see figure S5 for  $3$ ,  $3^-$ ,  $3^{2-}$ ).

orientations of the R groups. The most stable isomers for  $2^-$  and  $3^-$  both feature Fe–Fe bond elongation ( $2a^-$  and  $3a^-$ ), like  $1^-$ . It is noteworthy that unrotated conformers with a broken Fe–S bond are reciprocally found ( $2b^-$ , 2.8 kcal/mol less stable than  $2a^-$  and  $3b^-$ , 1.9 kcal/mol less stable than  $3a^-$ ) very close in energy. They feature a stabilising remote interaction between a H atom of a  $CH_2$  group of ethyl/benzyl substituents and the apical FeCO bond. As for  $1$ , the free energy gaps between rotated ( $2c^-$  and  $3c^-$ ) and unrotated ( $2a^-$  and  $3a^-$ ) isomers in mono-anionic species are significantly decreased compared to those calculated in the neutral forms (10.8 kcal/mol in  $2$  vs 3.7 kcal/mol in  $2^-$  and 10.5 kcal/mol in  $3$  vs 3.0 kcal/mol in  $3^-$ ). This follows the expected trend for the stabilisation of rotated isomers when increasing the steric hindrance of the dithiolate bridge.<sup>[75]</sup> As observed previously for  $1$ , the second reduction leads to isomers with one broken Fe–S bond and a CO group in bridging position ( $2a-b^{2-}$ ,  $3a-b^{2-}$ ). Various isomers of these dianions with different  $FeS_2CH_2CR_2$  conformations are within a relatively small energy gap ( $\sim 2$  kcal/mol).

Optimised geometries of the relevant neutral, mono-anionic and di-anionic species of  $1$ , possibly involved in the 2e-reduction pathways, are presented in Figure 7. The calculated redox potentials associated with the first and the second electron transfer involving the most stable  $1$ ,  $1^-$  and  $1^{2-}$  isomers, are predicted to be normally ordered and relatively close (0.07 V). The major structural change takes place during the second electron transfer which results in a kinetic constant  $k_{s(2)}$  smaller than that of the first electron transfer  $k_{s(1)}$ . These results are consistent with the experimentally observed potential compression leading to a two-electron wave at slow scan rates separated into two single-electron waves at higher scan rates. Finally, it should be noted that the redox potentials become inverted when the formation of  $1b^-$  as an intermediate species is considered. The non-prohibitive instability of  $1b^-$

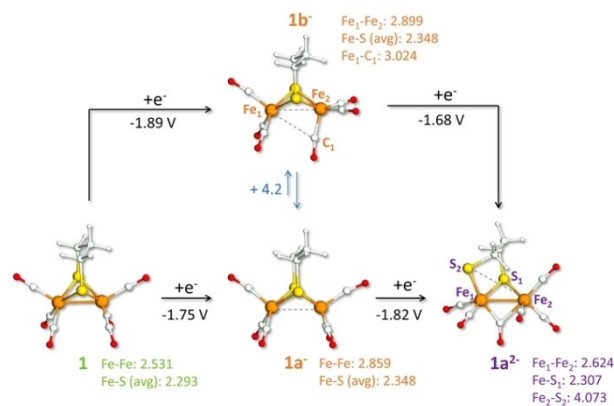
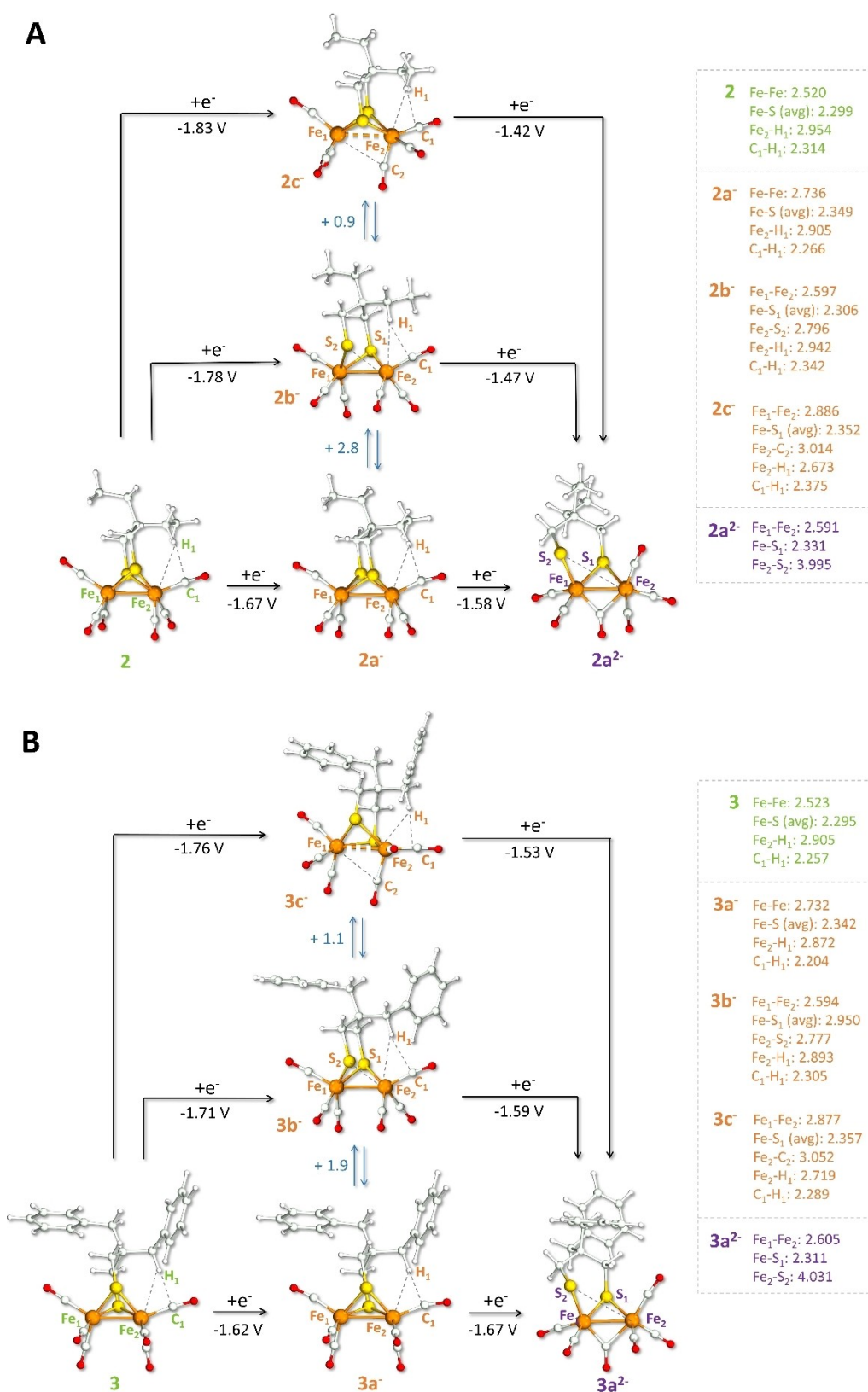


Figure 7. Optimised structures of the most relevant neutral, anionic, and dianionic species (selected bond distances, in Å, are reported in green (1), orange ( $1^-$ ), and purple ( $1^{2-}$ ). Redox potentials vs  $Fc^+/Fc$  are also reported (black values), together with  $\Delta G$  (in blue) among species with the same charge.

(which can be formed via  $1a^- \rightarrow 1b^-$  isomerisation with an activation barrier of 5.2 kcal/mol), alongside the precision limit of the employed (or any) DFT scheme in predicting  $\Delta G$  values, could therefore support the idea that some experimental circumstances may trigger the inversion of potentials. Complexes  $2$  and  $3$  behave differently than  $1$ . The CV of  $2$  shows, for all the scan rates, a two-electron process arising from a potential inversion without any possibility of discrimination. In the case of  $3$ , a two-electron transfer is also observed but the current function at high scan rates tends towards one electron. Optimised geometries of the most relevant neutral ( $2$ - $3$ ), mono-anionic ( $2^-$ ,  $3^-$ ) and di-anionic ( $2^{2-}$ ,  $3^{2-}$ ) species involved in the 2e-reduction pathways are considered in Figure 8. For  $2^-$ , the stretching of the Fe–Fe bond appears sufficient to lead to a



**Figure 8.** DFT optimised structures of the most relevant neutral (green), anionic (orange), and di-anionic (purple) species for complexes **2** (A) and **3** (B) (selected bond distances in Å; redox potentials vs Fc<sup>+/0</sup>/Fc (black values) and  $\Delta G$  (in blue) among species with the same charge).

potential inversion. The thermodynamically ( $\Delta G = 2.8$  kcal/mol) and kinetically ( $\Delta G^\ddagger = 3.3$  kcal/mol) accessible isomerisation of  $2a^-$  into  $2b^-$ , involving a broken Fe–S bond, as well as that leading to  $2c^-$  (inverted isomer) have also to be considered as supporting the inversion process. The experimental value of 2.7 found for the ratio between the current of the single step, reversible two-electron transfer, to the current of a reversible one-electron transfer determined at the lowest scan rates, strongly supports the assumption that there is a noticeable potential inversion.<sup>[99]</sup> Such an observation has been already made during the reduction of the azadithiolate complexes  $[\text{Fe}_2(\text{CO})_6(\mu\text{-(SCH}_2)_2\text{X})](\text{X}=\text{NR}, \text{R}=\text{CH}_2\text{CH}_2\text{OCH}_3, i\text{-Pr})$ .<sup>[54]</sup> Finally, whatever the reduced isomers considered, a potential inversion is predicted. The structures of the most stable neutral, mono-reduced and doubly-reduced forms of **3** are very similar to those of **2**. The calculated redox potentials associated to the first ( $3 \rightarrow 3a^-$ ) and the second ( $3a^- \rightarrow 3a^{2-}$ ) electron transfers involving the most stable  $3$ ,  $3^-$  and  $3^{2-}$  isomers are normal ordered and very close (Figure 8-B), which is inconsistent with experimental observations. However, the isomer  $3b^-$ , very close in energy (1.9 kcal/mol) to  $3a^-$ , could be quickly formed with an activation barrier of 3 kcal/mol. Its involvement in the reductive process better rationalises the observed inversion of the redox potentials. Furthermore, when considering the transient formation of  $3b^-$  after the first reduction at  $-1.62$  V ( $3 \rightarrow 3a^-$ ), the second reduction potential ( $3b^- \rightarrow 3a^{2-}$ ) is  $-1.59$  V and the half sum for the two electrons reduction,  $-1.605$  V, fits to the experimental potential of  $-1.61$  V. A pathway involving the energetically close isomer  $3c^-$  (with inverted geometry) is also consistent with an inversion of potential.

**3** behaves very similarly to the complexes  $[\text{Fe}_2(\text{CO})_6(\mu\text{-bdt})]$  ( $\text{bdt}=\text{S}_2\text{C}_6\text{H}_4$ ) (**4**)<sup>[56–57]</sup> and  $[\text{Fe}_2(\text{CO})_6(\mu\text{-edt})]$  ( $\text{edt}=\text{S}(\text{CH}_2)_2\text{S}$ )<sup>[72]</sup> with a current function decreasing from a two-electron transfer to a one-electron value without wave-splitting. This behaviour suggests that either structural rearrangements or the dismutation are quenched at high scan rates.

In the case of other complexes, such as  $[\text{Fe}_2(\text{CO})_6(\mu\text{-(SCH}_2)_2\text{S})]$  or  $[\text{Fe}_2(\text{CO})_6(\mu\text{-SCH}_2)_2(\text{Et})\text{P}=\text{O})]$ , involved in a two-electron-reduction process at the same potential, the wave-splitting has not been observed and the rate constant of the second electron transfer,  $k_{s(2)}$ , is larger than  $k_{s(1)}$ <sup>[65,100]</sup> while the two rate constants are close in the case of  $[\text{Fe}_2(\text{CO})_6(\mu\text{-bdt})]$ .<sup>[56–57]</sup> The structural modification of this latter complex upon electron transfer has been the subject of questioning.<sup>[63,101]</sup> For the sake of comparison, the reductive behaviours of  $[\text{Fe}_2(\text{CO})_6(\mu\text{-bdt})]$  were re-considered by DFT (see in Supporting Information and Figure S6). The results agree with a recent study which shows that an energetically favoured reduction pathway involves the cleavage of the Fe–S bond after the transfer of the first electron, in the mono-anionic intermediate without the bridging of a carbonyl.<sup>[101]</sup> The shift of one terminal carbonyl to a bridging position and an increase of about  $0.35$  Å of the Fe–Fe bond is observed after the second electron transfer.<sup>[102,103]</sup>

More in detail, the formation of a mono-anionic intermediate featuring a  $\mu\text{-CO}$ , previously proposed by Felton et al.<sup>[61]</sup> is predicted to be kinetically impeded<sup>[101]</sup> and thermodynamically disfavored, according to both our calculations and results in the

reference [101]. It is worth noting, however, that in both case studies ( $+1.8$  kcal/mol and  $0.6$  kcal/mol, respectively) thermodynamic gaps are so small that an unquestionable conclusion on the intimate mechanism of **4** reduction cannot be drawn.

The charge polarisation of a molecule is known to impact its interaction with the solvent and consequently the potential inversion.<sup>[22–25,104]</sup> Attempts to describe the charges repartition in the complexes **1–4** were performed in order to get additional information for rationalising the inversion of potentials. The localization of the charge(s) in the mono-anion and di-anion species and their solvation may impact the inversion of potential by decreasing the coulombic repulsion. The calculation of the atomic partial charges (calculated for molecular fragments) of neutral, anionic and di-anionic forms of complexes **2**, **3** and **4** were performed in order to know their distribution in such molecules. The atomic partial charge distribution (according to the NPA partition scheme of the electron density, see Computational Details) over the molecular fragments of **2**, **3** and **4** (Figure S7) reveals that most of the negative charge is stored by CO ligands. That is an expected trend showing the delocalization of the electron density on CO ligands upon the transfer of one and two electrons through  $\pi$ -backbonding from the metallic centres. The concerted decrease and increase of the atomic charges on the iron and sulfur atoms, respectively, upon cleavage of one Fe–S bond ( $4a^-$  vs  $4b^-$ ) is also consistent. The electron withdrawing properties of the group in the dithiolate bridge emphasise this trend, which also accords with the increase of the electron atomic charge in di-anionic species on benzyl and benzenedithiolate group, through their respective inductive or mesomeric effects. In fact, in the case of this study, dichloromethane is the sole solvent used and the separation of charges is expected to be limited considering the structure of these diiron complexes on the contrary of extended polymers.<sup>[104]</sup> Another observation emerging from the atomic partial charge analysis is a more extended delocalization of the electron over  $3a^-$  than  $2a^-$ , thanks to the benzyl based dithiolate scaffold. Indeed, a non-negligible fraction of electron density (ca 0.14 electrons, see Figure S7) is redistributed (upon reduction of the neutral forms) over the Bn based linker of  $3a^-$  but not in the Et based one of  $2a^-$  (Figure 8). This is as a factor that stabilises  $3a^-$  over  $2a^-$ , which is consistent with an easier-to-observe inversion of potentials in **2** vs **3**.

The nature of the species generated by the reaction of CO with the di-anion has been also investigated by DFT as well as the reaction pathways for CO binding at the di-anionic level (Figure 9). Reasonable dinuclear structures, arising from the formation of a di-anionic entity like the one mentioned in the literature for  $1^{2-}$ <sup>[54,98]</sup> were considered. The CO binding is energetically favoured for all the three species considered herein, with comparable values of the free energy of association. Among the geometries found for the CO-adducts of each system, two “types” of structures are energetically preferred:  $[\text{X-COa}]^{2-}$ , in which one sulfur atom is detached from both iron centres (see  $\Delta G_{\text{Xa}}$  values, Figure 9), and  $[\text{X-COb}]^{2-}$ , in which both sulfur atoms are linked to the same Fe centre (see  $\Delta G_{\text{Xb}}$  values, Figure 9). The former is energetically preferred to the

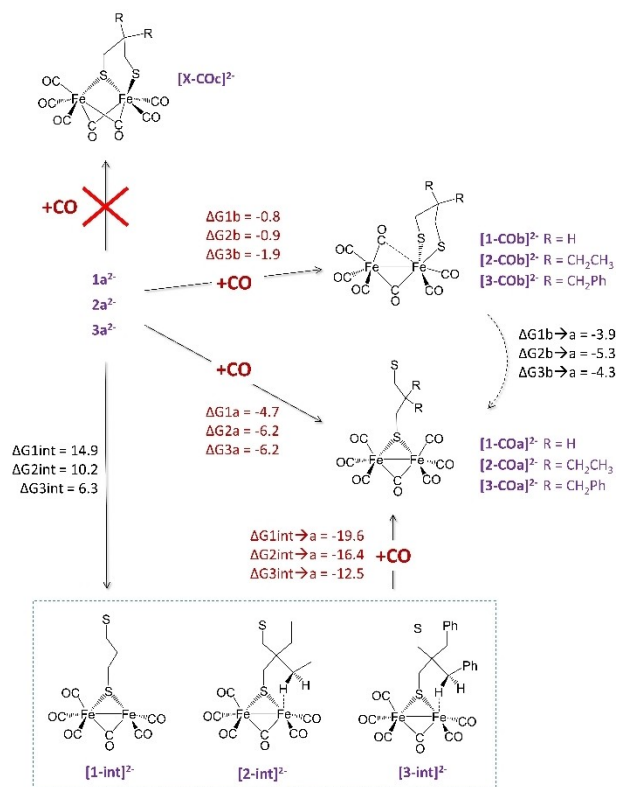


**Figure 9.** Structural hypotheses for the product arising from the reduction of  $1^{2-}$  under CO in  $\text{CH}_2\text{Cl}_2$ -[NBu<sub>4</sub>][PF<sub>6</sub>] and pathways for CO binding to  $1^{2-}$ ,  $2^{2-}$  and  $3^{2-}$  (free energies are in kcal/mol).  $\Delta G1$ ,  $\Delta G2$ , and  $\Delta G3$  are referred to reaction steps involving species 1, 2 and 3, respectively.

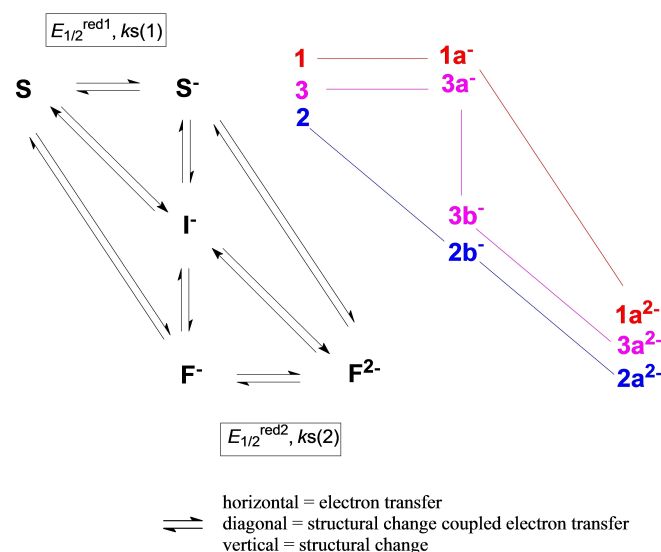
latter by  $\sim 4$ – $5$  kcal/mol (see  $\Delta GXb \rightarrow a$  values, Figure 9). Two mechanisms for  $[X-COa]^{2-}$  formation can be envisioned: a concerted process, in which the CO binding is concomitant with the unbinding of a sulfur atom (thus following  $\Delta GXa$  or  $\Delta GXb$ ), and a two-steps process, in which the sulfur atom dissociation from the metal precedes the CO binding (following  $\Delta GXint + \Delta GXint \rightarrow a$ ). A high activation barrier (26 kcal/mol) for the concerted process involving  $1^{2-}$  suggests that a two-step mechanism is more likely to occur. In such a process, an intermediate structure should form ( $[X-int]^{2-}$ ), whose nature alters the overall kinetics of the CO binding. Interestingly, in  $[2-int]^{2-}$  and  $[3-int]^{2-}$ , an agostic interaction between one  $-\text{CH}_2$  group of the dithiolate and the iron atom stabilizes the intermediate in the order  $[3-int]^{2-} > [2-int]^{2-} > [1-int]^{2-}$ , a trend that correlates with the steric hindrance of the dithiolate. We infer that the presence of such interaction may slow down CO association.

## Conclusion

As mentioned before, a two-electron transfer can be performed through a step-by-step (normal-ordering of potential) or a simultaneous transfer (potential inversion) depending on both the nature of the complexes and the medium. The simultaneous

transfer prevails when the stability of the di-anion is great and that of the anion is conversely low. The electrochemical results reported in this work may derive from the different pathways presented in scheme 1. In this scheme, S and F<sup>2-</sup> stand for geometries of the complexes 1–3 in their stable neutral (starting geometry) and di-anionic (final geometry) forms. The mono-anionic species S<sup>-</sup> and F<sup>-</sup> have the same geometries as S (with a slightly elongated Fe–Fe bond) and F<sup>2-</sup> (a broken Fe–S bond and an inverted conformation), respectively. I<sup>-</sup> arises from the isomerisation of S<sup>-</sup>. On the basis of DFT results, I<sup>-</sup> may have different geometries among which the most stable feature either a cleaved Fe–S bond or an inverted conformation. The conditions of the S<sup>-</sup>/I<sup>-</sup> equilibrium (vertical step in Scheme 1) may be more or less perturbed by a modification of the experimental conditions (solvent, ionic strength) and particularly the time scale of the experiment (scan rate). Whatever the geometry of I<sup>-</sup>, its reduction into F<sup>2-</sup> again implicates an isomerisation during the electron transfer. Therefore, a diagonal in Scheme 1 corresponds to a step where the isomerisation (structural change) and the electron transfer are concomitant. Moreover, one has to keep in mind that only the two most stable geometries of the mono-anion calculated by DFT have been considered in the discussion.

In the case of 1, the pathway  $S \rightarrow S^- \rightarrow F^{2-}$  is followed. The two-electron wave obtained at slow scan rates can be split in two one-electron steps at higher scan rates suggesting that the standard heterogeneous electron transfer rate  $k_{s(2)}$  is smaller than  $k_{s(1)}$ . This accords with a major structural change coupled with the second electron transfer. For 2, DFT calculations revealed that the pathway  $S \rightarrow S^- \rightarrow F^{2-}$  supports an inversion of potentials but the fact that the current function does not tend towards that corresponding to one-electron at high scan rates suggests that the two electron transfers have similar kinetics rates constants,  $k_{s(2)} \sim k_{s(1)}$  and that they are strongly coupled to the structural change that cannot be limited at fast scan rate,



**Scheme 1.** The different pathways for the mechanism of two electron reduction of 1–3.

which suggests that the pathway  $S \rightarrow I^- \rightarrow F^{2-}$  is followed. The pathway  $S \rightarrow S^- \rightarrow F^{2-}$  cannot be retained for **3** even if DFT predicts that it is favoured with the most stable species because this pathway is not consistent with the inversion of potentials, experimentally observed. Unlike **2**, the pathway  $S \rightarrow S^- \rightarrow I^- \rightarrow F^{2-}$  can be considered with an isomerisation process ( $S^- \rightarrow I^-$ ) that would be limited at high scan rates. The difference in the scan-rate dependence of the current functions observed for **2** and **3** suggests that, in the experimental conditions, in the case of **2**, the structural change is distributed over the two electron transfers (EE process) whereas for **3** the overall process is better described as a ECE mechanism with an isomerisation step  $S^- \rightarrow I^-$ , more separated from the electron transfer. Finally, the different situations reported in this study are due to the timing of the structural changes vs redox steps. The introduction of a bulky group in the bridgehead of the dithiolate linker has obviously an effect on normally ordered (as in **1**) or inverted (as in **2** and **3**) reduction potentials in the same experimental conditions. Despite the fact that Et  $\rightarrow$  Bn replacement is not predicted to significantly alter the overall geometry and energy of the most stable mono-reduced and bi-reduced forms, such a replacement alters the kinetics of the electron transfer vs the structural changes. Finally, the results herein illustrate that despite the fact that curves corresponding to a transfer of two electrons may appear very similar at first glance, intimate processes that rationalise these behaviours may be different. Moreover, it is worth noting that the di-iron systems, inspired by the H-cluster, which undergo a potential inversion are able to accumulate two electrons through an energetically more favourable pathway than a normally-ordered electron transfer. This process in itself is reminiscent of the biological principle of electronic bifurcation.<sup>[105–108]</sup> Another benefit of these systems undergoing inversion potential is that they may perform redox transformations of substrates with a lower energetical cost while keeping a favourable driving force. Understanding which molecular determinants govern the flexibility of the redox potentials of (multi)metallic coordination compounds is expected to reflect on how to target biomimicry with properly tailored potential inversion. This may be strategic for the future development of bioinspired transition metal-based electron bifurcating devices,<sup>[109–112]</sup> the question to know whether two-electron reduced di-iron systems may behave as such cofactors being open. Our contribution herein shows that the dithiolate bulk of diiron complexes can exert a subtle kinetic role in the modulation of the normal ordering vs inversion of redox potentials.

## Experimental Section

**Materials and methods:** All the syntheses of complexes **1–3** were carried out under an inert atmosphere, using Schlenk techniques. Solvents were deoxygenated and dried according to standard procedures.

2,2-dialkylpropane-1,3-dithiol,<sup>[113]</sup> complexes  $[Fe_2(CO)_6(\mu\text{-pdt}^{R2})]$ ,<sup>[78]</sup> were prepared according to reported procedure. <sup>1</sup>H NMR data of **3** were recorded at room temperature in CDCl<sub>3</sub> on a Bruker AMX 400 spectrometer of the 'Service général des plateformes, Université de

Brest' and referenced to SiMe<sub>4</sub>. The infrared spectra were recorded on a Perkin-Elmer spectrometer. Chemical analyses were made by the "Service de Microanalyse I.C.S.N.", Gif sur Yvette (France). Electrochemical measurements were conducted using a PG-STAT 128 N Autolab or a  $\mu$ -Autolab (type III) electrochemical analyser driven by the GPES software. All the electrochemical studies were carried out in a conventional three-electrode cell under an inert atmosphere (argon) or CO atmosphere. The preparation and the purification of the supporting electrolyte [NBu<sub>4</sub>][PF<sub>6</sub>] were as described previously.<sup>[114]</sup> The working electrode was a vitreous carbon disk of 0.3 cm in diameter, polished with alumina prior to use. A platinum wire was used as counter electrode. The reference electrode was an Ag|Ag<sup>+</sup> electrode, however, all the potentials (text, tables, and figures) are quoted against the (Fc<sup>+</sup>/Fc) couple; ferrocene was added as an internal standard at the end of the experiments.

Crystal data for **3** were collected on an Oxford Diffraction X-Calibur-2 CCD diffractometer, equipped with a jet cooler device and graphite-monochromated Mo–K $\alpha$  radiation ( $\lambda = 0.71073 \text{ \AA}$ ). The structure was solved and refined by standard procedures.<sup>[115]</sup>

Deposition Number 2224778 contains the supplementary crystallographic data for this paper. These data are provided free of charge by the joint Cambridge Crystallographic Data Centre and Fachinformationszentrum Karlsruhe Access Structures service.

**Computational (DFT) details:** Geometry optimizations have been carried out with the TURBOMOLE 7.4.1 suite of programs.<sup>[116]</sup> The BP86 functional of the electron density has been used in conjunction with a triple- $\zeta$  TZVP basis set,<sup>[117]</sup> in light of the suitability demonstrated by such a computational scheme in previous investigations regarding analogous complexes based on Fe/Ni-thiolate scaffolds.<sup>[118]</sup> Grimme's D3 corrections have been considered to account for dispersive interactions.<sup>[119]</sup> We took advantage of the Resolution-of-Identity (RI) technique to speed up calculations.<sup>[120]</sup> The solvent effect has been modelled implicitly according to the COSMO approach, by setting an  $\epsilon = 8.93$  of CH<sub>2</sub>Cl<sub>2</sub>.<sup>[121]</sup> Full vibrational analysis was performed on each optimised geometry to verify its nature as genuine stationary points, thus confirming that there were no imaginary frequencies for pure potential energy minima. A Natural Population Analysis (NPA) as implemented in the NBO program was performed to quantify atomic charges and spin densities. Free energies were derived from SCF energy values by estimating the various contributions (q-rotational, q-translational, q-vibrational) to the total partition function (Q), and assuming that Q can be evaluated as a product of such terms. Temperature and pressure were set to 298.15 K and 1 bar, respectively, to evaluate enthalpy and entropy contributions. The scaling factor for the SCF wavenumbers was set to 0.9914 (default value in TURBOMOLE). Redox potentials were obtained by evaluating the in-solvent free energy difference between reduced and oxidised species. The relation  $E^\circ = -\Delta G^\circ/nF$  ( $n$  = number of electrons involved in the redox process;  $F$  = Faraday constant) was used to calculate the absolute redox potential of the redox couple under investigation and of the reference couple Fc<sup>+</sup>/Fc (−4.98 V), calculated at the same level of theory.

**Preparation of  $[Fe_2(CO)_6(\mu\text{-(SCH}_2)_2\text{CBn}_2)]$  (**3**):** **3** has been already used as a precursor in a previous work,<sup>[122]</sup> but its preparation and spectroscopic and structural characterizations were not reported. A green mixture of Fe<sub>3</sub>(CO)<sub>12</sub> (1.50 g, 2.98 mmol) and dithiol (300 mg, 1.04 mmol) was stirred at 80 °C in 70 mL of toluene. The reaction was monitored by IR spectroscopy. After 3 h, the reaction solution was evaporated. The crude product was chromatographed on silica gel, with hexane as eluent. The first green band was excess of [Fe<sub>3</sub>(CO)<sub>12</sub>]. The second red band was eluted with a hexane/CH<sub>2</sub>Cl<sub>2</sub> (60/40) mixture and was collected. Yield: 0.4 g (66%). Diffraction-

quality crystals were obtained by slow diffusion of hexane in a dichloromethane solution of **3** at  $-20^{\circ}\text{C}$ . IR ( $\text{CH}_2\text{Cl}_2$ ): $\nu(\text{CO})$ :2073(s), 2033(vs) et 2001(s)  $\text{cm}^{-1}$ .  $^1\text{H}$  NMR (400 MHz,  $\text{C}_6\text{D}_6$ , 298 K)  $\delta$ :7.07–6.74 (m, 10H, 2  $\text{C}_6\text{H}_5$ ), 2.36 (s, 4H, 2  $\text{CH}_2\text{Ph}$ ), 1.92 (s, 4H, 2  $\text{SCH}_3$ ). Anal. Calcd for  $\text{Fe}_2\text{S}_2\text{C}_{23}\text{H}_{18}\text{O}_6$  (found): C, 48.79 (48.78) ; H, 3.20 (3.12).

## Acknowledgements

CNRS (Centre National de la Recherche Scientifique), the University of Brest (Université de Bretagne Occidentale), the University of Milano Bicocca are acknowledged for financial support. We are grateful to Dr Jean-François Capon, now retired, for his involvement in the experimental work and to Dr F. Michaud for the crystallographic measurements of **1**.

## Conflict of Interests

The authors declare no conflict of interest.

## Data Availability Statement

The data that support the findings of this study are available in the supplementary material of this article.

**Keywords:** bioinspired model of hydrogenases · DFT calculations · diiron complex · dithiolate bridge · inversion of potential

- [1] C. Tard, C. J. Pickett, *Chem. Rev.* **2009**, *109*, 2245–2274.
- [2] K. A. Vincent, A. Parkin, F. A. Armstrong, *Chem. Rev.* **2007**, *107*, 4366–4413.
- [3] C. J. Pickett, *J. Biol. Inorg. Chem.* **1996**, *1*, 601–606.
- [4] C. J. Pickett, K. A. Vincent, S. K. Ibrahim, C. A. Gormal, B. E. Smith, S. P. Best, *Chem. Eur. J.* **2003**, *9*, 76–87.
- [5] R. R. Schrock, *Angew. Chem. Int. Ed.* **2008**, *47*, 5512–5522; *Angew. Chem.* **2008**, *120*, 5594–5605.
- [6] D. V. Yandulov, R. R. Schrock, *Science* **2003**, *301*, 76–78.
- [7] H. Tanaka, H. Mori, H. Seino, M. Hidai, Y. Mizobe, K. Yoshizawa, *J. Am. Chem. Soc.* **2008**, *130*, 9037–9047.
- [8] Y. Tanabe, Y. Nishibayashi, *Coord. Chem. Rev.* **2013**, *257*, 2551–2564.
- [9] K. Arashiba, Y. Miyake, Y. Nishibayashi, *Nat. Chem.* **2011**, *3*, 120–125.
- [10] J. S. Anderson, J. Rittle, J. C. Peters, *Nature* **2013**, *501*, 84–87.
- [11] A. M. Appel, J. E. Bercaw, A. B. Bocarsly, H. Dobbek, D. L. DuBois, M. Dupuis, J. G. Ferry, E. Fujita, R. Hille, J. A. Kenis, C. A. Kerfeld, R. H. Morris, C. H. F. Peden, A. R. Portis, S. W. Ragsdale, T. B. Rauchfuss, J. N. H. Reek, L. C. Seefeldt, R. K. Thauer, G. L. Waldrop, *Chem. Rev.* **2013**, *113*, 6621–6658.
- [12] N. J. English, M. M. El-Hendawy, D. A. Mooney, J. M. D. MacElroy, *Coord. Chem. Rev.* **2014**, *269*, 85–95.
- [13] M. Beller, U. T. Bornscheuer, *Angew. Chem. Int. Ed.* **2014**, *53*, 4527–4528; *Angew. Chem.* **2014**, *126*, 4615–4617.
- [14] A. McSkimming, S. B. Colbran, *Chem. Soc. Rev.* **2013**, *42*, 5439–5488.
- [15] F. C. Anson, F. Ciardelli, K. Yamamoto, *Polymers Adv. Technol.* **1995**, *6*, 105–105.
- [16] J. Nomrowski, O. S. Wenger, *J. Am. Chem. Soc.* **2018**, *140*, 5343–5346.
- [17] H. Takeda, C. Cometto, O. Ishitani, M. Robert, *ACS Catal.* **2017**, *7*, 70–88.
- [18] K. Tanifuji, Y. Ohki, *Chem. Rev.* **2020**, *120*, 5194–5251.
- [19] S. Kallaene, A. W. Hahn, T. Weyhermueller, E. Bill, F. Neese, S. DeBeer, M. van Gastel, *Inorg. Chem.* **2019**, *58*, 5111–5125.
- [20] S. Navarro-Jaen, M. Virginie, J. Bonin, M. Robert, R. Wojcieszak, A. Y. Khodakov, *Nat. Chem. Rev.* **2021**, *5*, 564–579.
- [21] D. S. Polcyn, I. Shain, *Anal. Chem.* **1966**, *38*, 370–375.
- [22] D. H. Evans, K. Hu, *J. Chem. Soc. Faraday Trans.* **1996**, *92*, 3983–3990.
- [23] D. H. Evans, *Chem. Rev.* **2008**, *108*, 2113–2144.
- [24] D. H. Evans, *Acta Chem. Scand.* **1998**, *52*, 194–197.
- [25] C. Kraiya, D. H. Evans, *J. Electroanal. Chem.* **2004**, *565*, 29–35.
- [26] A. Nafady, T. T. Chin, W. E. Geiger, *Organometallics* **2006**, *25*, 1654–1663.
- [27] C. J. Adams, R. C. da Costa, R. Edge, D. H. Evans, M. F. Hood, *J. Org. Chem.* **2010**, *75*, 1168–1178.
- [28] F. A. Schultz, *J. Solid State Electrochem.* **2011**, *15*, 1833–1843.
- [29] R. L. Lord, F. A. Schultz, M.-H. Baik, *Inorg. Chem.* **2010**, *49*, 4611–4619.
- [30] D. Uhrhammer, F. A. Schultz, *J. Phys. Chem. A* **2002**, *106*, 11630–11636.
- [31] J. B. Fernandes, L. Q. Zhang, F. A. Schultz, *J. Electroanal. Chem.* **1991**, *297*, 145–161.
- [32] T. T. Chin, W. E. Geiger, A. L. Rheingold, *J. Am. Chem. Soc.* **1996**, *118*, 5002–5010.
- [33] D. T. Pierce, W. E. Geiger, *J. Am. Chem. Soc.* **1989**, *111*, 7636–7638.
- [34] D. T. Pierce, W. E. Geiger, *J. Am. Chem. Soc.* **1992**, *114*, 6063–6073.
- [35] A. J. Downard, A. M. Bond, A. J. Clayton, L. R. Hanton, D. A. McMorran, *Inorg. Chem.* **1996**, *35*, 7684–7690.
- [36] K. Lam, W. E. Geiger, *Org. Electrochem.* **2015**, 395–431.
- [37] M. D. Ryan, *J. Electrochem. Soc.* **1978**, *125*, 547–555.
- [38] N. A. Macias-Ruvalcaba, D. H. Evans, *J. Phys. Chem. B* **2005**, *109*, 14642–14647.
- [39] D. H. Evans, M. W. Lehmann, *Acta Chem. Scand.* **1999**, *53*, 765–774.
- [40] E. Gileadi, *J. Electroanal. Chem.* **2002**, *532*, 181–189.
- [41] M. W. Lehmann, P. Singh, D. H. Evans, *J. Electroanal. Chem.* **2003**, *549*, 137–143.
- [42] K. Hinkelmann, J. Heinze, *Ber. Bunsenges. Phys. Chem.* **1987**, *91*, 243–249.
- [43] A. J. Bard, L. R. Faulkner, *Electrochemical Methods. Fundamentals and Applications*, Wiley, New-York, **1980**, chapter 11, pp 429–485.
- [44] J.-M. Savéant, *Elements of Molecular and Biomolecular Electrochemistry - An Electrochemical Approach to Electron Transfer Chemistry*, Wiley, **2006**, ch. 2, pp 78–181.
- [45] C. Amatore, J. M. Savéant, *J. Electroanal. Chem.* **1978**, *86*, 227–232.
- [46] L. Schwartz, L. Eriksson, R. Lomoth, F. Teixidor, C. Vinas, S. Ott, *Dalton Trans.* **2008**, 2379–2381.
- [47] P. S. Singh, H. C. Rudbeck, P. Huang, S. Ezzaher, L. Eriksson, M. Stein, S. Ott, R. Lomoth, *Inorg. Chem.* **2009**, *48*, 10883–10885.
- [48] K. Charreter, M. Kdider, J.-F. Capon, F. Gloaguen, F. Y. Pétillon, P. Schollhammer, J. Talarmin, *Inorg. Chem.* **2010**, *49*, 2496–2501.
- [49] R. J. Wright, C. Lim, T. D. Tilley, *Chem. Eur. J.* **2009**, *15*, 8518–8525.
- [50] G. Qian, H. Wang, W. Zhong, X. Liu, *Electrochim. Acta* **2015**, *163*, 190–195.
- [51] J. Zhao, Z. Wei, X. Zeng, X. Liu, *Dalton Trans.* **2012**, *41*, 11125–11133.
- [52] R. J. Wright, W. Zhang, X. Yang, M. Fasulo, T. D. Tilley, *Dalton Trans.* **2012**, *41*, 73–82.
- [53] S. Wang, S. Pullen, V. Weippert, T. Liu, S. Ott, R. Lomoth, L. Hammarström, *Chem. Eur. J.* **2019**, *25*, 11135–11140.
- [54] J.-F. Capon, S. Ezzaher, F. Gloaguen, F. Y. Pétillon, P. Schollhammer, J. Talarmin, T. J. Davin, J. E. McGrady, K. W. Muir, *New J. Chem.* **2007**, *31*, 2052–2064.
- [55] F. Gloaguen, D. Morvan, J.-F. Capon, P. Schollhammer, J. Talarmin, *J. Electroanal. Chem.* **2007**, *603*, 15–20.
- [56] J.-F. Capon, F. Gloaguen, P. Schollhammer, J. Talarmin, *J. Electroanal. Chem.* **2004**, *566*, 241–247.
- [57] J.-F. Capon, F. Gloaguen, P. Schollhammer, J. Talarmin, *J. Electroanal. Chem.* **2006**, *595*, 47–52.
- [58] L. Chen, M. Wang, F. Gloaguen, D. Zheng, P. Zhang, L. Sun, *Inorg. Chem.* **2013**, *52*, 1798–1806.
- [59] L. Chen, M. Wang, F. Gloaguen, D. Zheng, P. Zhang, L. Sun, *Chem. Eur. J.* **2012**, *18*, 13968–13973.
- [60] X. Zhu, W. Zhong, X. Liu, *Int. J. Hydrogen Energy* **2016**, *41*, 14068–14078.
- [61] G. A. N. Felton, A. K. Vannucci, J. Chen, L. T. Lockett, N. Okumura, B. J. Petro, U. I. Zakai, D. H. Evans, R. S. Glass, D. L. Lichtenberger, *J. Am. Chem. Soc.* **2007**, *129*, 12521–12530.
- [62] L. Schwartz, P. S. Singh, L. Eriksson, R. Lomoth, S. Ott, *C. R. Chim.* **2008**, *11*, 875–889.
- [63] J. Chen, A. K. Vannucci, C. A. Mebi, N. Okumura, S. C. Borowski, M. Swenson, L. T. Lockett, D. H. Evans, R. S. Glass, D. L. Lichtenberger, *Organometallics* **2010**, *29*, 5330–5340.
- [64] S. Gao, J. Fan, S. Sun, F. Song, X. Peng, Q. Duan, D. Jiang, Q. Liang, *Dalton Trans.* **2012**, *41*, 12064–12074.

- [65] J. Windhager, M. Rudolph, S. Bräutigam, H. Görls, W. Weigand, *Eur. J. Inorg. Chem.* **2007**, 2748–2760.
- [66] U.-P. Apfel, D. Troegel, Y. Halpin, S. Tschierlei, U. Uhlemann, H. Görls, M. Schmitt, J. Popp, P. Dunne, M. Venkatesan, M. Coey, M. Rudolph, J. G. Vos, R. Tacke, W. Weigand, *Inorg. Chem.* **2010**, *49*, 10117–10132.
- [67] R. Trautwein, L. R. Almazahreh, H. Görls, W. Weigand, *Z. Anorg. Allg. Chem.* **2013**, *639*, 1512–1519.
- [68] M. H. Cheah, S. J. Borg, M. I. Bondin, S. P. Best, *Inorg. Chem.* **2004**, *43*, 5635–5644.
- [69] M. H. Cheah, S. J. Borg, S. P. Best, *Inorg. Chem.* **2007**, *46*, 1741–1750.
- [70] J. P. Collman, R. K. Rothrock, R. G. Finke, E. J. Moore, F. Rose-Munch, *Inorg. Chem.* **1982**, *21*, 146–156.
- [71] Y. Teramoto, K. Kubo, S. Kume, T. Mizuta, *Organometallics* **2013**, *32*, 7014–7024.
- [72] G. A. N. Felton, B. J. Petro, R. S. Glass, D. L. Lichtenberger, D. H. Evans, *J. Am. Chem. Soc.* **2009**, *131*, 11290–11291.
- [73] E. S. Donovan, G. S. Nichol, G. A. N. Felton, *J. Organomet. Chem.* **2013**, *726*, 9–13.
- [74] R. Goy, U.-P. Apfel, C. Elleouet, D. Escudero, M. Elstner, H. Görls, J. Talarmin, P. Schollhammer, L. González, W. Weigand, *Eur. J. Inorg. Chem.* **2013**, 4466–4472.
- [75] F. Arrigoni, F. Rizza, J. Vertemara, R. Breglia, C. Greco, L. Bertini, G. Zampella, L. De Gioia, *ChemPhysChem* **2020**, *21*, 2279–2292.
- [76] O. T. E. Selan, M. H. Cheah, B. F. Abrahams, R. W. Gable, S. P. Best, *Aust. J. Chem.* **2022**, *75*, 649–659.
- [77] Z. Xiao, W. Zhong, X. Liu, *Dalton Trans.* **2022**, *51*, 40–47.
- [78] M. L. Singleton, R. M. Jenkins, C. L. Klemashevich, M. Y. Darenbourg, *C. R. Chim.* **2008**, *11*, 861–874.
- [79] S. J. Borg, T. Behrsing, S. P. Best, M. Razavet, X. Liu, C. J. Pickett, *J. Am. Chem. Soc.* **2004**, *126*, 16988–16999.
- [80] S. P. Best, S. J. Borg, J. M. White, M. Razavet, C. J. Pickett, *Chem. Commun.* **2007**, 4348–4350.
- [81] D. Chong, I. P. Georgakaki, R. Mejia-Rodriguez, J. Sanabria-Chinchilla, M. P. Soriaga, M. Y. Darenbourg, *Dalton Trans.* **2003**, 4158–4163.
- [82] F. Barrière, N. Camire, W. E. Geiger, U. T. Mueller-Westerhoff, R. Sanders, *J. Am. Chem. Soc.* **2002**, *124*, 7262–7263.
- [83] F. Barrière, W. E. Geiger, *J. Am. Chem. Soc.* **2006**, *128*, 3980–3989.
- [84] W. E. Geiger, F. Barrière, *Acc. Chem. Res.* **2010**, *43*, 1030–1039.
- [85] P.-Y. Orain, J.-F. Capon, F. Gloaguen, P. Schollhammer, J. Talarmin, *Int. J. Hydrogen Energy* **2010**, *35*, 10797–10802.
- [86] S. Muratsugu, K. Sodeyama, F. Kitamura, S. Tsukada, M. Tada, S. Tsuneyuki, H. Nishihara, *Chem. Sci.* **2011**, *2*, 1960–1968.
- [87] M. K. Harb, A. Daraosheh, H. Görls, E. R. Smith, G. J. Meyer, M. T. Swenson, T. Sakamoto, R. S. Glass, D. L. Lichtenberger, D. H. Evans, M. El-khateeb, W. Weigand, *Heteroat. Chem.* **2014**, *25*, 592–606.
- [88] A. Hildebrandt, D. Miesel, Q. Yuan, J. Freytag, J. Mahrholdt, H. Lang, *Dalton Trans.* **2019**, *48*, 13105–13494.
- [89] E. J. Lyon, I. P. Georgakaki, J. H. Reibenspies, M. Y. Darenbourg, *J. Am. Chem. Soc.* **2001**, *123*, 3268–3278.
- [90] R. Trautwein, L. R. Almazahreh, H. Görls, W. Weigand, *Dalton Trans.* **2015**, *44*, 18780–18794.
- [91] The parameters  $i_p$  and  $E_p$  are respectively the peak current and the peak potential of a redox process;  $E_{1/2} = (E_p^a + E_p^c)/2$ ;  $E_p^a$ ,  $i_p^a$  and  $E_p^c$ ,  $i_p^c$  are respectively the potential and the current of the anodic and of the cathodic peak of a reversible process;  $\Delta E_p = E_p^a - E_p^c$ . CV stands for cyclic voltammetry;  $v$  ( $V s^{-1}$ ) is the scan rate in CV experiments.
- [92] D. Chouffai, G. Zampella, J.-F. Capon, L. De Gioia, A. Le Goff, F. Y. Pétillon, P. Schollhammer, J. Talarmin, *Organometallics* **2012**, *31*, 1082–1091.
- [93] The diffusion coefficient,  $D_0$ , of  $[Fe_2(CO)_6(\mu-(SCH_2)_2CH_2)]$  was calculated from the current of the first reduction peak ( $i_p^{red1}$ ) for  $v > 5 V/s$ , when the two reduction steps of the complex are well separated (see Figure),  $D_0 = 6.6 \times 10^{-6} cm^2/s$ . The diffusion coefficient of  $[Fe_2(CO)_4(\kappa^2-LL)(\mu-(SCH_2)_2CH_2)]$  ( $LL = I_{Me}-CH_2-I_{Me}$ ,  $I_{Me} = 1$ -methylimidazol-2-ylidene) was taken in Ref. [92].
- [94] the  $(i_p^a/i_p^c)^{red}$  peak current ratio was calculated following the method of Nicholson, see R. S. Nicholson, *Anal. Chem.* **1966**, *38*, 1406.
- [95] S. Ezzaher, J.-F. Capon, F. Gloaguen, F. Y. Pétillon, P. Schollhammer, J. Talarmin, *Inorg. Chem.* **2007**, *46*, 9863–9872.
- [96] A. Darchen, H. Mousser, H. Patin, *J. Chem. Soc. Chem. Commun.* **1988**, 968–970.
- [97] S. J. Borg, J. W. Tye, M. B. Hall, S. P. Best, *Inorg. Chem.* **2007**, *46*, 384–394.
- [98] C. Greco, G. Zampella, L. Bertini, M. Bruschi, P. Fantucci, L. De Gioia, *Inorg. Chem.* **2007**, *46*, 108–116.
- [99] J. Heinze, *Angew. Chem. Int. Ed. Engl.* **1984**, *23*, 831–847.
- [100] L. R. Almazahreh, F. Arrigoni, H. Abul-Futouh, M. El-khateeb, H. Görls, C. Elleouet, P. Schollhammer, L. Bertini, L. De Gioia, M. Rudolph, G. Zampella, W. Weigand, *ACS Catal.* **2021**, *11*, 7080–7098.
- [101] J. P. H. Oudsen, B. Venderbosch, D. J. Martin, T. J. Korstanje, J. N. H. Reek, M. Tromp, *Phys. Chem. Chem. Phys.* **2019**, *21*, 14638–14645.
- [102] M. Mirmohades, S. Pullen, M. Stein, S. Maji, S. Ott, L. Hammarström, R. Lomoth, *J. Am. Chem. Soc.* **2014**, *136*, 17366–17369.
- [103] S. Wang, A. Aster, M. Mirmohades, R. Lomoth, L. Hammarström, *Inorg. Chem.* **2018**, *57*, 768–776.
- [104] P. Hapiot, L. D. Kispert, V. V. Kononov, J.-M. Savéant, *J. Am. Chem. Soc.* **2001**, *123*, 6669–6677.
- [105] W. Buckel, R. K. Thauer, *Chem. Rev.* **2018**, *118*, 3862–3886.
- [106] J. L. Yuly, C. E. Lubner, P. Zhang, D. N. Beratan, J. W. Peters, *Chem. Commun.* **2019**, *55*, 4091.
- [107] J. L. Yuly, P. Zhang, C. E. Lubner, J. W. Peters, D. N. Beratan, *PNAS* **2020**, *117*, 21045–21051.
- [108] K. Kayastha, S. Vitt, W. Buckel, U. Ermler, *Arch. Biochem. Biophys.* **2021**, *701*, 108796.
- [109] N. Chongdar, K. Pawlak, O. Rüdiger, E. J. Reijerse, P. Rodríguez-Maciá, W. Lubitz, J. A. Birrell, H. Ogata, *J. Biol. Inorg. Chem.* **2020**, *25*, 135–149.
- [110] J. W. Peters, D. N. Beratan, G. J. Schut, M. W. W. Adams, *Chem. Commun.* **2018**, *54*, 4091.
- [111] A. Das, C. Hessin, Y. Ren, M. Desage-El Murr, *Chem. Soc. Rev.* **2020**, *49*, 8840–8867.
- [112] C. Hessin, J. Schleinitz, N. Le Breton, S. Choua, L. Grimaud, V. Fourmond, M. Desage-El Murr, C. Léger, *Inorg. Chem.* **2023**, *62*, 3321–3332.
- [113] V. K. Aggarwal, I. W. Davies, R. Franklin, J. Maddock, M. F. Mahon, K. C. Molloy, *J. Chem. Soc.-Perkin Trans.* **1994**, *1*, 2363–2368.
- [114] F. Arrigoni, S. Mohamed Bouh, C. Elleouet, F. Y. Pétillon, P. Schollhammer, L. De Gioia, G. Zampella, *Chem. Eur. J.* **2018**, *24*, 15036–15051.
- [115] a) L. J. Farrugia, WinGX suite for small-molecule single-crystal crystallography, *J. Appl. Crystallogr.* **1999**, *32*, 837–838; b) L. J. Farrugia, WinGX and ORTEP for Windows: an update, *J. Appl. Crystallogr.* **2012**, *45*, 849–854.
- [116] R. Ahlrichs, M. Bär, M. Häser, H. Horn, C. Kölmel, *Chem. Phys. Lett.* **1989**, *162*, 165–169.
- [117] a) A. D. Becke, *Phys. Rev. A* **1988**, *38*, 3098–3100; b) J. P. Perdew, *Phys. Rev. B* **1986**, *33*, 8822–8824; c) A. Schäfer, C. Huber, R. Ahlrichs, *J. Chem. Phys.* **1994**, *100*, 5829–5835.
- [118] a) L. Chatelain, J.-B. Breton, F. Arrigoni, P. Schollhammer, G. Zampella, *Chem. Sci.* **2022**, *13*, 4863–4873; b) G. M. Chambers, T. B. Rauchfuss, F. Arrigoni, G. Zampella, *Organometallics* **2016**, *35*, 836–846; c) S. Siculo, M. Bruschi, L. Bertini, G. Zampella, G. Filippi, F. Arrigoni, L. De Gioia, C. Greco, *Int. J. Hydrogen Energy* **2014**, *39*, 18565–18573.
- [119] a) S. Grimme, J. Antony, S. Ehrlich, H. Krieg, *J. Chem. Phys.* **2010**, *132*, 154104–154122; b) S. Grimme, S. Ehrlich, L. Goerigk, *J. Comput. Chem.* **2011**, *32*, 1456–1465.
- [120] K. Eichkorn, F. Weigend, O. Treutler, R. Ahlrichs, *Theor. Chem. Acc.* **1997**, *97*, 119–24.
- [121] a) A. Klamt, *J. Phys. Chem.* **1995**, *99*, 2224–2235; b) A. Klamt, *J. Phys. Chem.* **1996**, *100*, 3349–3353.
- [122] A. Hobballah, R. Motei, S. Lounissi, C. Elleouet, F. Y. Pétillon, P. Schollhammer, *Eur. J. Inorg. Chem.* **2021**, 205–216.

Manuscript received: February 21, 2023  
Accepted manuscript online: April 4, 2023  
Version of record online: May 19, 2023